SEMARAK ILMU PUBLISHING

Journal of Advanced Research in Applied Sciences and Engineering Technology

Journal homepage:
https://semarakilmu.com.my/journals/index.php/applied_sciences_eng_tech/index
ISSN: 2462-1943

Fractional Flow Reserve of Non-Newtonian Blood Flow in a Stenosed Bifurcated Artery

Kannigah Thirunanasambantham[1], Siti Nor Hasimah Hamid[1], Zuhaila Ismail[1,*], Lim Yeou Jiann[1], Amnani Shamjuddin[2], Yahaya Shagaiya Daniel[3]

[1] Department of Mathematical Sciences, Faculty of Science, Universiti Teknologi Malaysia, 81310, Malaysia
[2] Chemical Reaction Engineering Group (CREG), Faculty of Chemical and Energy Engineering, Universiti Teknologi Malaysia, 81310, Malaysia
[3] Department of Mathematical Sciences, Faculty of Science, Kaduna State University, Nigeria

ARTICLE INFO

Article history:
Received 1 January 2026
Received in revised form 20 January 2026
Accepted 25 January 2026
Available online 7 February 2026

Keywords:
Fractional flow reserve (FFR); magnetohydrodynamic; hybrid nanofluid; bifurcated artery; stenosis

ABSTRACT

Coronary artery stenosis alters blood flow, increasing the risk of myocardial ischemia. This study explores the impact of four plaque formations on fractional flow reserve in a bifurcated artery using COMSOL Multiphysics. Blood is modelled as a non-Newtonian fluid via a generalised power-law, with rigid arterial walls representing diseased vessels. Hybrid nanofluids and magnetohydrodynamic effects are included. Under hyperemic conditions, pressure gradients across stenosed regions are analysed to compute fractional flow reserve. Results show that plaque geometry and distribution significantly affect fractional flow reserve: simpler bifurcations maintain higher fractional flow reserve, while complex geometries reduce and destabilise it. Magnetic fields help stabilise flow and slightly improve fractional flow reserve in narrowed areas. Hybrid nanofluids enhance fractional flow reserve in wider vessels but may reduce it in tighter regions due to increased viscosity. These findings support the integration of advanced fluid models and electromagnetic effects for more accurate cardiovascular diagnostics.

1. Introduction

Cardiovascular diseases (CVD), especially coronary artery disease (CAD), are the leading cause of death globally. CAD results from atherosclerosis, which narrows the coronary arteries and can lead to heart attacks. Doctors assess the severity of stenosis using fractional flow reserve (FFR), which compares blood flow through a stenosis to normal flow [1]. While FFR values traditionally guide stent implantation, research suggests that minor FFR reductions may not require revascularisation, as medical therapy can be effective. This conservative approach offers promising management options for patients with stable CAD and insignificant FFR values [1].

Researchers are utilising imaging data from CT, MRI, and computational fluid dynamics (CFD) to create patient-specific arterial geometries for finite element simulations [2]. These simulations calculate velocity and pressure fields in coronary vessels, allowing for the derivation of fractional flow reserve (FFR) values. Normal FFR values are around 1.0, while values below 0.75–0.80 indicate significant stenosis and potential revascularisation needs [3]. The use of CFD for FFR assessment is

* *Corresponding author.*
E-mail address: zuhaila@utm.my

efficient and cost-effective, providing precise evaluations of arterial stenosis [3]. Yan *et al.,* [4] demonstrated how CFD can assess myocardial ischemia, while Fandaros *et al.,* [5] evaluated FFR using patient-specific coronary artery geometries in COMSOL Multiphysics, simplifying complex geometries and enhancing diagnostic accuracy.

Bifurcated arteries complicate blood flow dynamics and the effects of stenosis, particularly near the bifurcation, thereby increasing the risk of ischemia and cardiac issues [6]. FFR is key for assessing stenosis, as it compares pressure in the affected artery to aortic pressure during peak flow, providing insight into the severity of blockages that traditional imaging may not reveal. Modelling blood flow in stenosed arteries is more precise when blood is treated as a non-Newtonian fluid, with the generalised power-law (GPL) model excelling in this regard [7]. It adjusts to varying shear rates, behaving like a Newtonian fluid at low rates and a power-law fluid at higher ones. Research shows that the GPL model enhances the accuracy of wall shear stress (WSS) and pressure distribution, identifying areas prone to plaque buildup and thrombosis [7].

Magnetohydrodynamics (MHD) further optimises this modelling by utilising blood's conductive properties. Magnetic fields generate Lorentz forces that alter velocity and pressure gradients, impacting FFR assessments [8]. Studies highlight that MHD effects are more pronounced in smaller and stenotic arteries, offering potential advancements in treating cardiovascular issues like hypertension and improving FFR estimations essential for coronary artery disease interventions [6].

This study examines hybrid nanofluids (HNF) of gold (Au) and silver (Ag) nanoparticles for modelling MHD blood flow in stenosed bifurcated arteries. HNFs improve thermal and rheological properties, with Au providing stability and Ag enhancing thermal conductivity and antimicrobial effects [9]. Al-Kouz *et al.,* [10] developed an HNF model that improves cardiovascular diagnostics, while Vaidya *et al.,* [11] showed magnetic fields enhance flow resistance, aiding targeted drug delivery. Overall, HNFs offer better hemodynamic control than mono-nanofluids, advancing non-invasive cardiovascular therapies. Research on bifurcated arterial geometries is limited, despite their vulnerability to atherosclerosis due to the presence of junctions and curvatures. Flow disturbances, such as reversal and stagnation, near bifurcations significantly impact hemodynamics [10]. This study analyses FFR in four configurations of stenosed bifurcated arteries, focusing on constrictions of 48%, 64%, and 84% in cross-sectional area [12].

The novelty of this work lies in the integration of MHD and HNF into a simulation framework to analyse their combined effects on pressure gradients and flow dynamics in blood vessels. By comparing FFR values with and without these influences, the study examines how electromagnetic control and nanoparticle-enhanced properties impact blood flow in diseased vessels. Blood is modelled as a non-Newtonian fluid to capture shear-dependent viscosity, with rigid arterial walls due to cholesterol-induced stiffening. The findings provide insights into non-invasive medical interventions, such as targeted drug delivery and flow regulation, thereby enhancing the understanding of hemodynamics in bifurcated arteries and offering new strategies for managing cardiovascular disease.

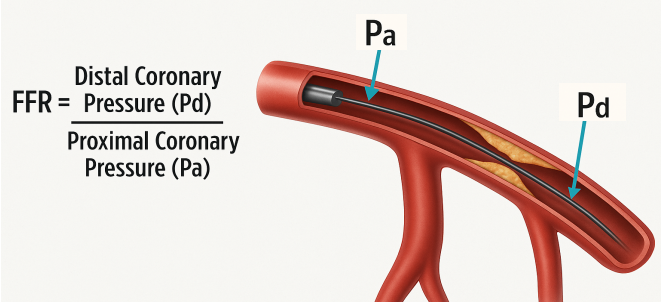

Fig. 1 The concept of fractional flow reserve [5]

2. Mathematical Formulation

Four distinct types of stenosis in a bifurcated artery are considered. To establish the computational domain for a stenosed bifurcated artery, several assumptions are made [13,14]:

(a) The artery is of finite length; four morphological types (Type I to Type IV) are defined, as depicted in Fig. 2
(b) The curvatures are introduced at lateral junctions and the flow divider to prevent discontinuities and separation zones.
(c) Stenosis shapes are typically irregular rather than uniform.

The proposed classifications are: Type I for healthy bifurcated arteries with no stenosis; Type II for stenosis near the bifurcation in the parent artery; Type III for stenosis extending to the upper wall of the bifurcation; and Type IV for stenosis in the parent vessel's proximal region and ostium. This framework, adapted from Zain *et al.,* [13] ranges from healthy to diseased bifurcated arteries.

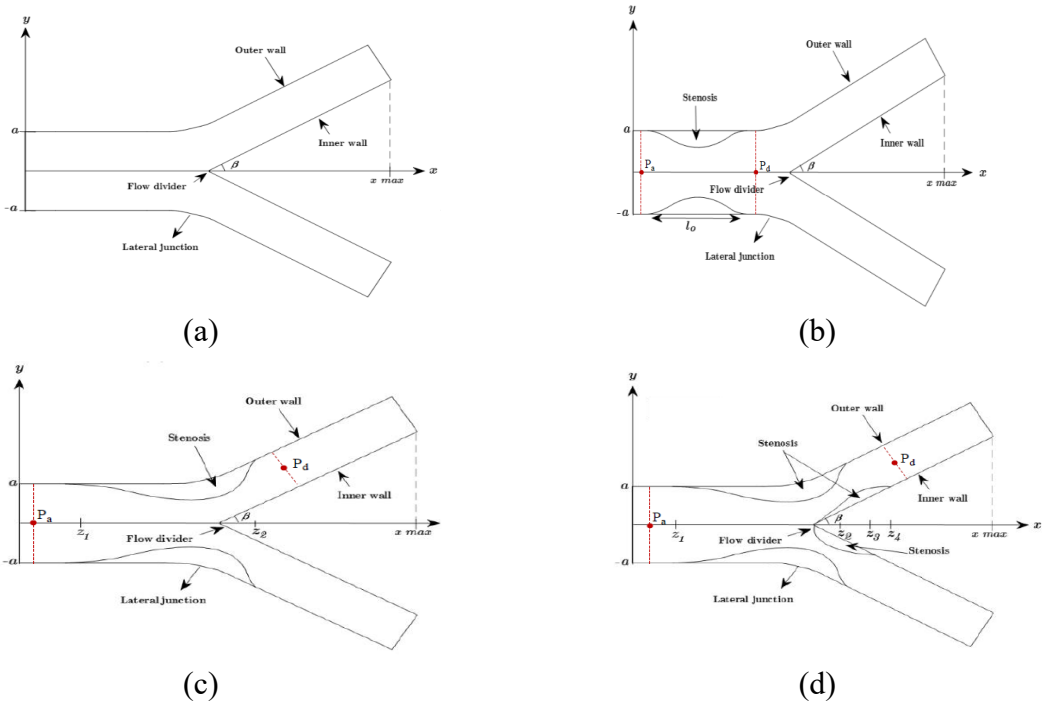

Fig. 2 Different model geometries of stenosed bifurcated artery, (a) Type I, (b) Type II, (c) Type III and (d) Type IV

This study examines the steady, incompressible flow of a GPL fluid in a stenosed bifurcated artery across four morphological configurations. An external magnetic field and the effects of HNF influence the flow. Dimensionless governing equations for the fluid flow are formulated as [13,14],

$$\frac{\partial u}{\partial x}+\frac{\partial v}{\partial y}=0 \tag{1}$$

$$u\frac{\partial u}{\partial x}+v\frac{\partial u}{\partial y}=-\frac{\partial p}{\partial x}+\frac{1}{\mathrm{Re}}\left(\frac{\rho_f}{\rho_{hnf}}\right)\left\{\left|\left[2\left(\frac{\partial u}{\partial x}\right)^2+2\left(\frac{\partial v}{\partial y}\right)^2+\left(\frac{\partial v}{\partial x}+\frac{\partial u}{\partial y}\right)^2\right]^{1/2}\right|^{n-1}\right\}\left(\frac{\partial^2 u}{\partial x^2}+\frac{\partial^2 u}{\partial y^2}\right)-\frac{M^2}{\mathrm{Re}}\left(\frac{\sigma_{hnf}}{\sigma_f}\right)\left(\frac{\rho_f}{\rho_{hnf}}\right)u, \tag{2}$$

$$u\frac{\partial v}{\partial x}+v\frac{\partial v}{\partial y}=-\frac{\partial p}{\partial y}+\frac{1}{\mathrm{Re}}\left(\frac{\rho_f}{\rho_{hnf}}\right)\left\{\left|\left[2\left(\frac{\partial u}{\partial x}\right)^2+2\left(\frac{\partial v}{\partial y}\right)^2+\left(\frac{\partial v}{\partial x}+\frac{\partial u}{\partial y}\right)^2\right]^{1/2}\right|^{n-1}\right\}\left(\frac{\partial^2 v}{\partial x^2}+\frac{\partial^2 v}{\partial y^2}\right). \tag{3}$$

where the parameters Re and *M* denote the Reynolds number and the Hartmann number, respectively, and is defined as [14,15],

$$\mathrm{Re}=\frac{\rho_f h}{mU_0^{n-2}} \text{ and } M=B_0\left(\frac{\sigma_f h^{n+1}}{mU_0^{n-1}}\right)^{1/2} \tag{4}$$

Dimensionless quantities describe the ratio of inertial to viscous forces and the influence of magnetic fields on fluid motion. Velocity components *u* and *v* relate to the *x* and *y* axes, while *p* denotes fluid pressure. The density of blood is represented by ρ_f, and ρ_{hnf} indicates the density of the fluid (blood) and HNF respectively. Electrical conductivities are denoted by σ_f for blood and σ_{hnf} for HNF. Parameter *m* indicates fluid consistency, and *n*, set at 1.2 in this study, signifies shear-thickening behaviour consistent with the GPL model [13,14]. U_0 is the reference velocity based on the study by Chakravarty *et al.,* [16]. Below is the boundary conditions of the problem is specified as below [13,14],

$$\text{Inlet}: u(x,y)=\frac{3}{2}\left(1-\left(\frac{y}{1/2}\right)^{\frac{n+1}{n}}\right), v(x,y)=0, \text{ at } x=0 \text{ and } -\frac{1}{2}\le y\le\frac{1}{2}. \tag{5}$$

$$\text{Outlet}: (-p\mathbf{I}+\tau)\cdot\mathbf{n}=0,$$

$$\text{Inner and Outer Walls}: u_{inner\ wall}=u_{outer\ wall}=0,\ v_{inner\ wall}=v_{outer\ wall}=0,$$

n is the outward unit normal vector, and **I** is the identity matrix. The thermophysical characteristics of the base fluid (blood) (*f*), along with Au and Ag nanoparticles and HNF formulated from these components, are detailed in Hussain *et al*., [17]. In this context, ϕ_{Ag} and ϕ_{Au} correspond to the

respective volume concentrations of silver and gold nanoparticles. The subscript *nf* is used to indicate quantities associated with the nanofluid mixture.

3. Validation and Mesh Test

Model validation was performed to ensure that the numerical simulation developed using COMSOL is correctly implemented and functioning as intended. To verify the reliability of the simulation, a mesh dependency test was done using the geometrical parameters from the benchmark model proposed by Zain *et al.* [13]. Simulations of blood as a Newtonian fluid were conducted at magnetic field strengths of 0 T, 8 T, 16 T, and 32 T, and validated against Zain *et al.,* [13]. Table 1 details the domain elements for each mesh configuration and the maximum velocity, U_{max}. Strong agreement was found, particularly for Mesh 3 and Mesh 4, with a minimal difference of about 0.0003 m/s. Discrepancies may stem from transient flow behaviour and validation methods. Mesh 4 was selected for further simulations to optimise accuracy and computational efficiency.

Table 1
Comparison of various meshes with different magnetic parameters *B*

Mesh	Domain elements	U_{max}			
		B			
		0T	8T	16T	32T
1	3429	0.5559	0.5193	0.4657	0.5359
2	5854	0.5598	0.5276	0.4802	0.5577
3	7332	0.5682	0.5397	0.5027	0.4711
4	17201	0.5711	0.5440	0.5093	0.4845
Zain *et al.,* [13]		0.5716	0.5439	0.5088	0.4842

4. Fractional Flow Reserve

Pressure profiles for bifurcated artery geometries (Type I to IV) were analysed along the central horizontal axis from inlet to outlet. Proximal pressure was extracted just before the stenosed region, while distal pressure was obtained immediately after. FFR is calculated as the ratio of mean distal pressure to mean aortic pressure, serving as an index to evaluate the severity of coronary artery stenosis. The severity of stenosis, S, is defined by the ratio of diameters at the narrowed region ($d_{stenosis}$) and the healthy segment (d_{normal}) of the artery using the expression of ($S=1-\alpha$) [18].

In the context of FFR analysis, the narrowing degree α ranges from 1 for a healthy artery with no stenosis to 0 for complete occlusion. Notably, Type III and Type IV have stenosis at the bifurcation, but α changes only at the mother artery, similar to Type II. A red line at FFR = 0.80 marks the clinically accepted threshold for recommending coronary intervention [18].

5. Results and Discussion

Figure 3(a) illustrates the relationship between FFR and stenosis severity across three bifurcated artery geometries: Type II, Type III, and Type IV. Type I is excluded from this analysis as it represents a normal bifurcation without stenosis, making variations in α irrelevant. The results indicate distinct FFR patterns for each geometry. Type II demonstrates a steep, non-linear FFR increase, exceeding the 0.80 threshold around $\alpha = 0.6$, which aligns with the S-shaped dependence [18]. In contrast, Type III shows a linear FFR progression that remains below 0.80 even at $\alpha = 1$, primarily due to reduced

distal pressure at the daughter artery caused by localised flow resistance. This suggests that relying solely on FFR may be inadequate, necessitating the use of additional metrics, such as the Pythagorean companion FFR_C or direct pressure measurements [18].

Type IV exhibits a complex, non-monotonic FFR curve, characterised by an initial rise, a dip, and a gradual recovery, indicating intricate flow dynamics that may be due to recirculation zones or pressure anomalies.

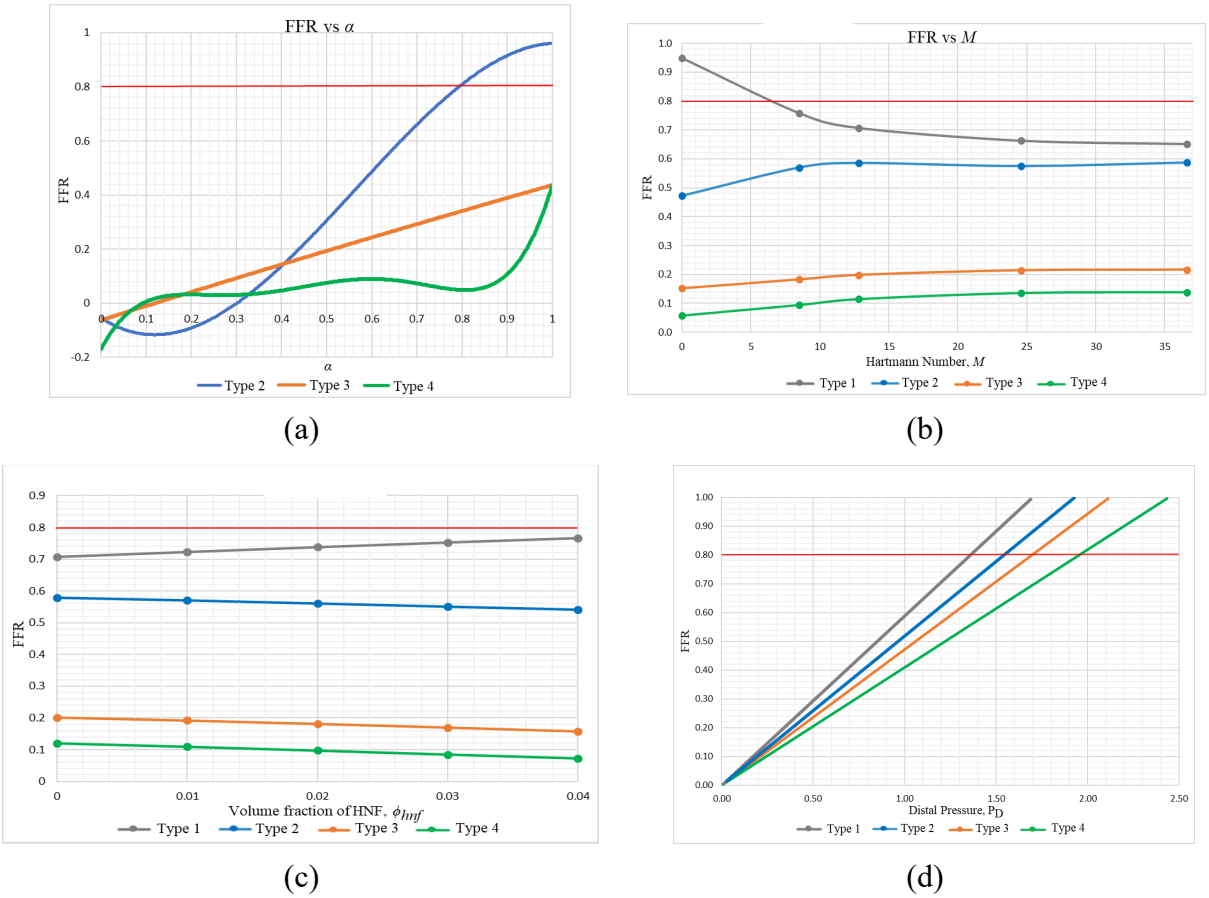

Fig. 3 Different model geometries of stenosed bifurcated artery (a) FFR vs. the severity of stenosis, α, (b) FFR vs. varying Hartmann number, *M*, (c) FFR vs. volume fraction of HNF, ϕ_{hnf} and (d) FFR vs. distal pressure, P_d

Like Type III, FFR for Type IV stays below 0.80, underscoring the high-risk nature of this geometry and the potential need for intervention based on anatomical features.

Figure 3(b) examines the impact of MHD on FFR in four bifurcated artery geometries (Type I-IV) with a constant HNF concentration of 0.01. The Hartmann number, *M*, varied from 0 to 36.6 to assess its effects on flow dynamics and perfusion. Type I, representing a healthy bifurcation, begins with an FFR near 0.90 at *M* = 0 due to natural pressure losses from the artery's branching and flow disturbances, even without stenosis. Similar findings were reported in previous studies where non-stenosed arteries showed FFR values under one due to geometric complexities [6,19]. As *M* increases, FFR gradually declines for Type I due to the Lorentz force, which increases flow resistance and pressure drop.Type II, with an initial FFR of 0.5-0.6, exhibits relative stability across the *M* range, indicating less sensitivity to changes in flow resistance from the magnetic field. In contrast, Types III and IV, which start with lower FFR values (around 0.15-0.2 and 0.05-0.1, respectively), exhibit a slight increase in FFR as *M* rises. This may suggest that the magnetic field stabilises disturbed flow patterns,

promoting smoother flow and improving perfusion modestly. Despite these improvements, Types III and IV remain below the clinical threshold of 0.80 across all *M* values, raising questions about the overall benefits of MHD. However, the observed increase in FFR implies that MHD could offer hemodynamic advantages by mitigating turbulence and promoting more uniform flow. Therefore, evaluating MHD's effectiveness should extend beyond just achieving an FFR of 0.80 to include improvements in blood flow characteristics, which may potentially reduce the need for invasive interventions.

Figure 3(c) explores the impact of varying the volume fraction of the HNF on FFR across four bifurcated artery geometries, labelled Type I to IV, under a constant MHD condition with a *M* of 12.8. The analysis reveals that as the volume fraction increases from 0 to 0.04, there are notable changes in coronary perfusion, which is the delivery of oxygen-rich blood to the myocardium. In Type I geometry, which represents healthy arteries, FFR remains stable with a slight increase as the volume fraction rises. This increase can be attributed to the enhanced thermal conductivity and improved energy transport properties of the nanofluid, which in turn improve flow dynamics. In contrast, Type II shows a slight decline in FFR with higher concentrations of HNF. The presence of stenosis alters flow dynamics and introduces geometric constraints that increase viscous resistance. Although HNF improves thermal conductivity, the constant temperature boundary conditions imply that thermal effects are less impactful, allowing mechanical resistance to dominate.

Types III and IV are characterised by severe anatomical constraints and lower baseline FFR values. In these cases, FFR consistently declines as the volume fraction of HNF increases. The increased viscosity and density of the nanofluid at higher concentrations exacerbate flow resistance in these already compromised vessels. Previous studies suggest that higher nanoparticle concentrations in stenosed arteries lead to elevated pressure gradients and reduced perfusion efficiency due to increased viscous drag [18,20]. These findings suggest that while HNF can provide modest enhancements in simpler artery geometries, its application in stenosed or anatomically complex configurations may require careful optimisation to avoid counterproductive effects. Overall, the results highlight the potential of HNF and MHD as non-invasive methods for flow control. They could improve both the predictability and uniformity of perfusion in challenging anatomical regions.

Figure 3(d) illustrates the linear relationship between FFR and distal pressure across stenosed segments for four bifurcated artery geometries (Type I through Type IV) under constant MHD of 12.8 and HNF of 0.01. Pressure values were assessed along the artery's centerline from inlet to outlet (refer to Fig. 2), with distal pressure chosen just downstream of the stenosis, where blood flow stabilises. This approach reflects the true post-stenotic pressure under hyperemic conditions, enabling accurate FFR calculations.

The data show that FFR increases linearly with distal pressure across all artery geometries. A higher distal pressure indicates reduced resistance through the narrowed segment, suggesting better perfusion. Conversely, low distal pressure signifies significant pressure loss due to stenosis, resulting in diminished FFR, often below the clinical threshold of 0.80, which raises concerns about myocardial perfusion and ischemia risk. In Type I, the line graph has the steepest slope, indicating that small increases in distal pressure result in notable improvements in FFR, a characteristic of a healthy artery where flow is laminar. Type II exhibits moderate sensitivity, showing gradual increases in FFR with pressure, indicating mild resistance and effective perfusion.

Types III and IV display shallower slopes, suggesting that, despite increased distal pressures, FFR remains low due to complex bifurcations or significant narrowing. Flow disturbances, such as turbulence, limit pressure recovery, resulting in FFR values that may not reach the clinical threshold, highlighting the impact of anatomical factors. In conclusion, the graph emphasises the role of distal pressure in modulating FFR and the varying responses of different geometries to pressure changes.

While MHD and HNF aid in flow stabilisation and pressure distribution, their effectiveness is limited by the artery's structural characteristics. These observations reinforce that FFR is both geometry-sensitive and pressure-dependent, advocating for a comprehensive assessment approach that incorporates anatomical and hemodynamic factors in evaluating coronary stenosis.

6. Conclusion

The study analyses FFR across four bifurcated artery geometries influenced by varying stenosis severity, MHD effects, and HNF volume fractions. Key findings include,

(a) Type I Geometry: Exhibits the highest FFR values and a steep response to distal pressure changes, indicating healthy perfusion.
(b) Type II Geometry: Shows a steep, non-linear FFR increase with stenosis severity, reflecting high sensitivity to moderate stenosis.
(c) Type III Geometry: Displays a linear but limited FFR response, suggesting constrained pressure recovery.
(d) Type IV Geometry: Has a consistently low FFR profile, indicating severe perfusion.

MHD effects reveal a gradual FFR decline in Type I with increased magnetic resistance, while Types III and IV show slight improvements. HNF analysis indicates that Types I and II maintain stable FFR values, whereas Types III and IV decline with increasing nanofluid concentration due to increased viscosity. A linear relationship between FFR and pressure drops is noted across all geometries. Overall, integrating MHD and HNF into cardiovascular modelling enhances perfusion, indicating that advanced fluid engineering can optimise therapeutic interventions in complex arterial geometries.

Acknowledgment

This work was supported by the Ministry of Higher Education Malaysia under the Fundamental Research Grant Scheme (FRGS) (FRGS/1/2022/TK05/UTM/02/11) and Universiti Teknologi Malaysia (UTM), UTM Fundamental Research Vote No: Q.J130000.3854.23H57.

References

[1] Firus Khan, Al'aina Yuhainis, Anis Safura Ramli, Suraya Abdul Razak, Noor Alicezah Mohd Kasim, Yung-An Chua, Ahmad Zia Ul-Saufie, Mohd Amin Jalaludin, and Hapizah Nawawi. "The M ala y sian HE alth and Well B eing A ssessmen T (MyHEBAT) Study Protocol: An Initiation of a National Registry for Extended Cardiovascular Risk Evaluation in the Community." *International journal of environmental research and public health* 19, no. 18 (2022): 11789. https://doi.org/10.3390/ijerph191811789

[2] Saveljic, Igor, Tijana Djukic, Dalibor Nikolic, Smiljana Djorovic, and Nenad Filipovic. "Numerical simulation of fractional flow reserve in atherosclerotic coronary arteries." In *2021 IEEE 21st International Conference on Bioinformatics and Bioengineering (BIBE)*, pp. 1-4. IEEE, 2021. https://doi.org/10.1109/BIBE52308.2021.9635457

[3] Gonnah, Ahmed R., Ahmed K. Awad, Ahmed E. Helmy, Ahmed B. Elsnhory, Omar Shazly, Saad A. Abousalima, Aser Labib, Hussein Saoudy, Ayman K. Awad, and David H. Roberts. "Comparing FFR-Guided Complete Revascularization and Conservative Management for Non-Culprit Lesions in STEMI Patients With Multivessel Disease: A Systematic Review and Meta-Analysis." *Catheterization and Cardiovascular Interventions* 105, no. 3 (2025): 633-642. https://doi.org/10.1002/ccd.31379

[4] Yan, Qing, Deqiang Xiao, Yaosong Jia, Danni Ai, Jingfan Fan, Hong Song, Cheng Xu, Yining Wang, and Jian Yang. "A multi-dimensional CFD framework for fast patient-specific fractional flow reserve prediction." *Computers in Biology and Medicine* 168 (2024): 107718. https://doi.org/10.1016/j.compbiomed.2023.107718

[5] Fandaros, Marina, Chloe Kwok, Zachary Wolf, Michael Shearer, Johnathan Scheiner, Yulee Li, J. Jane Cao, and Wei Yin. "Left coronary artery biomechanics: a characterization study using fluid structure interaction simulations." *Biomechanics and Modeling in Mechanobiology* (2025): 1-16. https://doi.org/10.1007/s10237-025-01974-3

[6] Kumar, Devendra, B. Satyanarayana, Rajesh Kumar, Sanjeev Kumar, and Narendra Deo. "Application of heat source and chemical reaction in MHD blood flow through permeable bifurcated arteries with inclined magnetic field in tumor treatments." *Results in Applied Mathematics* 10 (2021): 100151. https://doi.org/10.1016/j.rinam.2021.100151

[7] Zain, Norliza Mohd, Zuhaila Ismail, and Peter Johnston. "A Stabilized Finite Element Formulation of Non-Newtonian Fluid Model of Blood Flow in A Bifurcated Channel with Overlapping Stenosis." *Journal of Advanced Research in Fluid Mechanics and Thermal Sciences* 88, no. 1 (2021): 126-138. https://doi.org/10.37934/arfmts.88.1.126139

[8] Gandhi, Rishu, B. K. Sharma, Qasem M. Al-Mdallal, and H. V. R. Mittal. "Entropy generation and shape effects analysis of hybrid nanoparticles (Cu-Al2O3/blood) mediated blood flow through a time-variant multi-stenotic artery." *International Journal of Thermofluids* 18 (2023): 100336. https://doi.org/10.1016/j.ijft.2023.100336

[9] Thirunanasambantham, K., Z. Ismail, Y. J. Lim, A. Shamjuddin, and Y. S. Daniel. "Computational simulation of MHD blood-based hybrid nanofluid flow through a stenosed artery." *Journal of Advanced Research in Numerical Heat Transfer* 28, no. 1 (2024): 145-164. https://doi.org/10.37934/arnht.28.1.145164

[10] Al-Kouz, Weal, Aissa Abderrahmane, M. D. Shamshuddin, Obai Younis, Sahnoun Mohammed, O. Anwar Bég, and Davood Toghraie. "Heat transfer and entropy generation analysis of water-Fe3O4/CNT hybrid magnetic nanofluid flow in a trapezoidal wavy enclosure containing porous media with the Galerkin finite element method." *The European Physical Journal Plus* 136, no. 11 (2021): 1-23. https://doi.org/10.1140/epjp/s13360-021-02192-3

[11] Vaidya, Hanumesh, Rajashekhar Choudhari, Fateh Mebarek-Oudina, and Kerehalli Vinayaka Prasad. "Computational Elucidation of Electromagnetic Effects on Peristaltic Nanofluid Transport in Microfluidics: Intersections of CFD, Biomedical and Nanotechnology Research." https://doi.org/10.37934/cfdl.16.11.3759

[12] Zain, Norliza Mohd, Zuhaila Ismail, Muhammad Sabaruddin Ahmad Jamali, and Yeou Jiann Lim. "Wall shear stress distribution of non-Newtonian blood flow in stenosed bifurcated artery." *Matematika* (2023): 75-86. https://doi.org/10.11113/matematika.v39.n1.1452

[13] Zain, Norliza Mohd, and Zuhaila Ismail. "Modelling of Newtonian blood flow through a bifurcated artery with the presence of an overlapping stenosis." *Malaysian Journal of Fundamental and Applied Sciences* 13, no. 2017 (2017): 304-309. https://doi.org/10.11113/mjfas.v13n4-1.866

[14] M. Xenos and E. Tzirtzilakis, "MHD Effects on Blood Flow in a Stenosis Department of Mathematics Technological Educational Institute of Western Greece," no. May, 2016.

[15] Thirunananasambantham, Kannigah, Zuhaila Ismail, Lim Yeou Jiann, and Amnani Shamjuddin. "Computational analysis of hybrid GPL blood nanofluid flow over various stenosed arteries in the presence of a magnetic field." *Alexandria Engineering Journal* 129 (2025): 598-611. https://doi.org/10.1016/j.aej.2025.06.046

[16] Chakravarty, S., and P. K. Mandal. "Mathematical modelling of blood flow through an overlapping arterial stenosis." *Mathematical and computer modelling* 19, no. 1 (1994): 59-70. https://doi.org/10.1016/0895-7177(94)90116-3

[17] Hussain, Azad, Lubna Sarwar, Aysha Rehman, Sobia Akbar, Fehmi Gamaoun, Hasan Huseyin Coban, Abdulrazak H. Almaliki, and Maram S. Alqurashi. "Heat transfer analysis and effects of (silver and gold) nanoparticles on blood flow inside arterial stenosis." *Applied sciences* 12, no. 3 (2022): 1601. https://doi.org/10.3390/app12031601

[18] Faes, Theo JC, Romain Meer, Guy R. Heyndrickx, and Peter LM Kerkhof. "Fractional flow reserve evaluated as metric of coronary stenosis—a mathematical model study." *Frontiers in Cardiovascular Medicine* 6 (2020): 189. https://doi.org/10.3389/fcvm.2019.00189

[19] Edrisnia, Hadis, Mohammad Hossein Sarkhosh, Bahram Mohebbi, Seyed Ehsan Parhizgar, and Mona Alimohammadi. "Non-invasive fractional flow reserve estimation in coronary arteries using angiographic images." *Scientific Reports* 14, no. 1 (2024): 15640. https://doi.org/10.1038/s41598-024-65626-9